

CONCEPT STUDY OF A FAST VTOL-UAV TECHNOLOGY- DEMONSTRATOR FOR MUM-T

Alexander Štrbac, German Aerospace Center (DLR), Braunschweig, Germany
Andreas E. Voigt, German Aerospace Center (DLR), Braunschweig, Germany
Daniel H. Greiwe, German Aerospace Center (DLR), Braunschweig, Germany
Peter Weiland, German Aerospace Center (DLR), Braunschweig, Germany
Rainer Bartels, German Aerospace Center (DLR), Braunschweig, Germany

Matthias Müller, Airbus Helicopters Technik GmbH (AHTech), Calden, Germany
Jörg Schmiedel, Airbus Helicopters Technik GmbH (AHTech), Calden, Germany
Martin Meunier, Airbus Helicopters Technik GmbH (AHTech), Calden, Germany
Uwe T. P. Arnold, Airbus Helicopters Technik GmbH (AHTech), Calden, Germany
Jörg Litzba, Airbus Helicopters Technik GmbH (AHTech), Calden, Germany

Abstract

The Manned Unmanned Teaming (MUM-T) of rotorcraft offers the potential to increase the effectivity and survivability of the combined tactical unit. Currently, commercially available Unmanned Aerial Vehicles (UAVs) with Vertical Take-Off and Landing (VTOL) capability are not specifically designed for fast forward flight and would slow down the entire tactical unit. This study presents the first results of the development of a technology-demonstrator with a maximum airspeed of at least 180 kt. The investigation of different VTOL-UAV concepts, the selection of a thrust-compound configuration and the first details of the predesign are described. Furthermore, the flight performance is analyzed with focus on maximum airspeed, power, endurance and range. The results show, that the proposed design of the VTOL-UAV is expected to fulfill the requirements.

1. INTRODUCTION

The formation of tactical units, which consist of manned and unmanned aircraft, offers the potential to increase the effectivity and survivability in future missions. For those Manned Unmanned Teaming (MUM-T) scenarios, the Unmanned Aerial Vehicle (UAV) can be used to increase the sensor perimeter of the manned aerial vehicle and thus provides re-

connaissance and threat detection. However, commercially available UAVs with Vertical Take-Off and Landing (VTOL) capability are currently not specifically designed for fast forward flight, neither by their configuration nor by their flight control system. Thus, UAVs have to be improved to fly significantly faster, if they shall accompany manned helicopters operating at high-speed [1]. To solve this issue, the project FaUSt (Fast Unmanned Scout) has been initiated, which is a collaboration between the German Aerospace Center (DLR) and the Airbus Helicopters Technik GmbH (AHTech) and is funded by the German Federal Office of Bundeswehr Equipment, Information Technology and In-Service Support (BAAINBw L1.1). The aim of the project is the design of a technology-demonstrator with sufficient maximum airspeed and the demonstration of flight control architectures for a compounded high-speed flight configuration by flight tests with DLR's modified superARTIS UAV [2].

At the moment, the Armed Forces of Germany operate the attack helicopter Tiger, the utility helicopter

Copyright Statement

The authors confirm that they, and/or their company or organization, hold copyright on all of the original material included in this paper. The authors also confirm that they have obtained permission, from the copyright holder of any third-party material included in this paper, to publish it as part of their paper. The authors confirm that they give permission, or have obtained permission from the copyright holder of this paper, for the publication and distribution of this paper as part of the ERF proceedings or as individual offprints from the proceedings and for inclusion in a freely accessible web-based repository.

NH90 and the cargo helicopter CH-53, which is expected to be replaced by the CH-47 Chinook. Depending on the mission equipment, those helicopters feature a maximum airspeed of approximately 160-170 kt. For the proposed MUM-T scenario, the VTOL-UAV is expected to leave the formation flight with the manned helicopter and to fly ahead in an unknown hostile environment. Therefore, the authors defined a maximum airspeed of at least 180 kt (≈ 93 m/s) as the primary design objective. Furthermore, the capability of the combined tactical unit to hover in cover of the terrain should not be limited by a poor hover efficiency of the VTOL-UAV.

Figure 1-1 shows an overview of currently available VTOL-UAVs with the focus on maximum airspeed (V_{Max}) and a notable Maximum Takeoff Weight (m_{MTOW}), which correlates to the potential mass of payload and fuel. A variety of slow and light weight VTOL-UAVs have been excluded from the overview, because they do not fit in the proposed scenario. The vertical reference lines indicate maximum airspeed of the Tiger and the NH90 helicopter. As depicted, commercially available products (circle) are designed in a helicopter configuration and are limited to a maximum airspeed of roughly 120 kt.

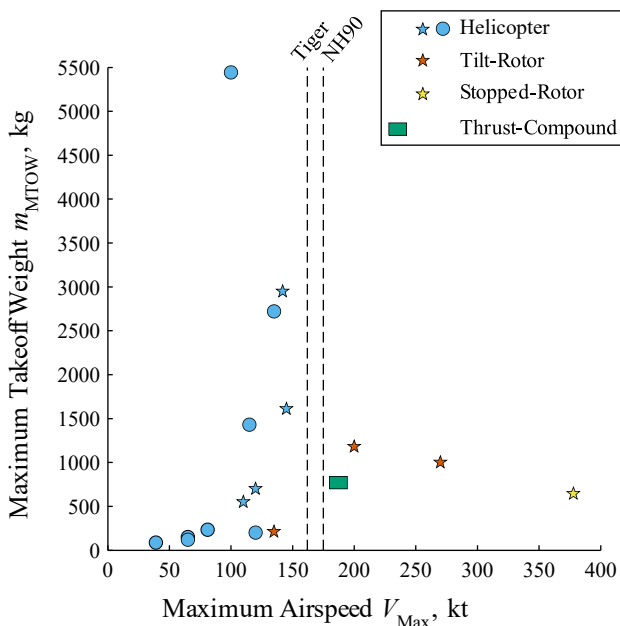


Figure 1-1: Overview of currently available VTOL-UAVs and the expected solution area of the FaUSt-Demonstrator (commercial product (circle), demonstrator or prototype (star))

Furthermore, technology-demonstrators and prototypes (star), which already have performed first flight, are added to Figure 1-1. Note that compari-

sons with those aircraft must be taken with care. Depending on the level of development, those aircraft may only focus on key technologies (endurance, attitude, airspeed, etc.) and may not possess the full capability of a commercial product. As depicted, the technology-demonstrators and prototypes in helicopter configuration fly slightly faster than the commercial products (e.g. [3], [4]). But only a very few have shown sufficient airspeed to potentially operate with current helicopters by using complex configurations with a high technological effort (tilt-rotor, e.g. ([5], [6]), stopped-rotor, e.g. [7]).

The focus of the new VTOL-UAV design of this study is to develop a technology-demonstrator, which is able to effectively operate in the proposed scenario with a minimum of technological effort and which is suitable for manufacturing in a potential follow-up project. Therefore, particular attention is paid on the balance between required flight performance and the availability and complexity of the utilized technology. As discussed in the next section, a thrust-compound configuration has been selected and the expected solution area is drawn in Figure 1-1 (green area).

This paper presents the first results of the development process. Firstly, a short overview of known fast VTOL configurations is given. Based on this research, a reference and two candidate configurations are defined and their expected flight performance is analyzed. Afterwards, the selection of a configuration for the FaUSt-Demonstrator is described. Secondly, a description of the system architecture and the design of the most important subsystems of the FaUSt-Demonstrator is given. Thirdly, the flight performance is analyzed in regards to maximum airspeed, power, endurance and range. Finally, the results are discussed and a conclusion is given.

2. CONCEPT INVESTIGATION

Several configurations have been used to combine fast flight and VTOL capabilities. Vectored-thrust fixed-wing aircraft (e.g. Hawker Siddeley Harrier, [8]) or vectored-thrust fixed-wing with additional lift engines (e.g. Dornier Do 31, [8]) belong to the fastest known aircraft configurations with VTOL capability, but suffer from a very poor hover efficiency and a complex transition flight phase. Tilt-wing (e.g. Ling-Temco-Vought XC-142, [8], [9]) and tilt-rotor configurations (e.g. Bell Boeing V-22 Osprey, [8], [9], [10]) can easily fulfill the airspeed requirement, but still

suffer from a comparably poor hover efficiency and a complex transition flight phase. The thrust-compound (e.g. Sikorsky X2, [9]) and lift-compound configurations (e.g. Eurocopter X³, [9]) are between conventional helicopters and tilt-rotor/tilt-wing configurations with a good to fair hover efficiency and without a complex transition flight phase. Last but not least, there are also rather exotic aircraft configurations known such as tail-sitter (e.g. Lockheed XFV-1, [8]) or stopped-rotor configurations (e.g. Sikorsky X-Wing, [8], [9]), both with a complex transition flight phase.

2.1. Candidates

For the further investigations, one single conventional helicopter configuration (baseline) and two different thrust-compound configurations have been defined (Figure 2-1 - Figure 2-3). All configurations feature a good hover efficiency, but only the thrust-compound configurations are expected to fulfill the maximum airspeed of at least 180 kt. Note that to take into account simulation uncertainties and to give a substantial speed margin, the maximum airspeed for the simulations is set to 194 kt (≈ 100 m/s).

Based on empirical data and the availability of turboshaft engines, the mass and the dimensions of the candidates have been estimated (Table 1). The disc loading was set to 350 N/m², which is suitable for small helicopters and UAVs. In combination with a MTOW of 700 kg, this results in a rotor diameter of approximately 5.0 m. With respect to the intended airspeed of 100 m/s the constant tip speed of the rotor was set to 200 m/s, which results in a potential advance ratio of 0.5. Neglecting the shape of the blade tip and the angle of attack of the rotor disc, the theoretical tip Mach number could reach 0.88.

Table 1: Overview of design parameters of the candidates and the resulting maximum airspeed

Candidate	0	1	2
MTOW, kg	700	700	700
Rotor diameter, m	5.0	5.0	5.0
Rotor solidity	0.13	0.11	0.11
Disk loading, N/m ²	350	350	350
Equivalent drag area, m ²	0.27	0.27	0.27
Maximum airspeed, kt	167	194	194
Maximum airspeed, m/s	86	100	100

Due to the large increase of the required total power at high-speed and the strong impact of the engine size on the fuselage shape for UAVs, a rather high equivalent drag area of 0.27 m² is chosen. The design parameters remain the same for the performance estimations of the candidates and the resulting maximum airspeeds are summarized in Table 1.

The conventional helicopter configuration, denoted as Candidate 0, is used as a baseline case for comparisons (Figure 2-1). It consists of a single main rotor, which provides lift and propulsion, and a tail rotor, which provides anti-torque and yaw-control. The main rotor of the conventional Candidate 0 must overcome weight and drag force. To prevent rotor stall, the blade loading was reduced by a moderate solidity of 0.13 in connection with a five-blade main rotor.

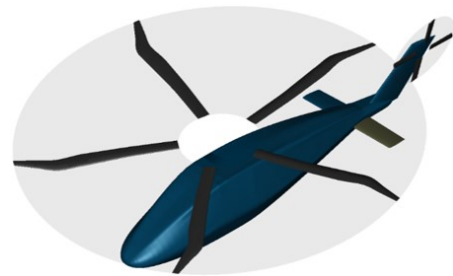


Figure 2-1: Candidate 0 - Conventional Helicopter

Candidate 1 represents a basic thrust-compound configuration and consists of a main rotor, a tail rotor and a pusher propeller (Figure 2-2). Therefore, main and tail rotor provide lift, anti-torque and propulsion in low-speed. In mid to high-speed, the propulsion is provided mainly by the pusher propeller and the main rotor is partially unloaded. The design of a five bladed main rotor has been considered to be avoided, because the fitting on the rather small dimensions of the technology-demonstrator would be complicated. With respect to the reduced thrust of the main rotor, the solidity is reduced to 0.11 with four main rotor blades.

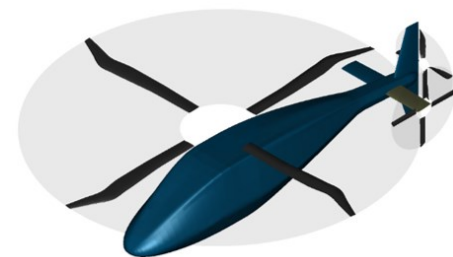


Figure 2-2: Candidate 1 - Thrust-Compound

Candidate 2 combines an intermeshing Flettner-Rotor with inherent anti-torque and a pusher propeller (Figure 2-3). Therefore, the unloading of the main rotor is similar to Candidate 1 at mid to high-speed. Comprising the discs to one results in the same parameters for the rotor with 350 N/m^2 and a solidity of 0.11.



Figure 2-3: Candidate 2 - Flettner-Thrust-Compound

2.2. Evaluation

DLR's design environment for rotorcraft IRIS (Integrated Rotorcraft Initial Sizing, [11], [12]) was used for initialization and modelling the candidates. Beyond the scope of the project FaUSt, IRIS features comprehensive sizing, including mission simulation, propulsion modelling and further analysis. However, the additional design effort has been considered not appropriate due to the project focus on a technology-demonstrator and the partial limitation on existing technology. With respect to the more sophisticated flight envelope, all flight performance computations were conducted with HOST (Helicopter Overall Simulation Tool, [13]). HOST is a comprehensive rotorcraft simulation program developed by Airbus Helicopters (formerly Eurocopter). It has been integrated into the IRIS design environment, enabling the flight model generation of different configurations by design rules and computation with alternative trim laws directly out of the process.

Figure 2-4 shows the result of the trim calculations for the horizontal forward flight of the candidates. As usual, the total power (P_{TOT}) is driven by the induced power of the main rotor at hover and by parasitic power of the fuselage at high-speed. The decrease of the induced power and the increase of the parasitic power with the airspeed causes a power minimum at mid-speed, which can be potentially used for maximum maneuver power. Apparently, the required installed power is determined by the high-speed flight and not the hover flight due to the airspeed requirement of the VTOL-UAV. Overall, Candidate 0 reaches a maximum airspeed of roughly 86 m/s ,

before the main rotor stalls and an equilibrium condition is not achievable anymore. Therefore, this baseline candidate is expected to miss or with intensive optimization barely reach the airspeed requirement.

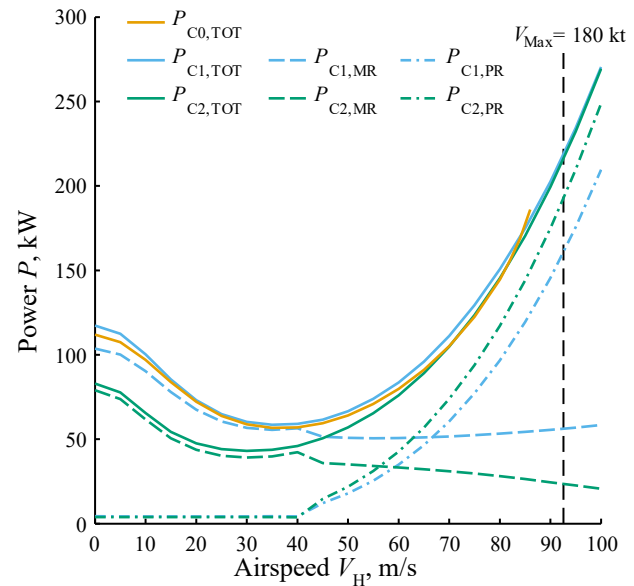


Figure 2-4: Forward flight performance of the candidates (total power (P_{TOT}), power main rotor (P_{MR}), power pusher (P_{PR}))

For the two thrust-compound configurations, the pusher propeller is in idle until the minimum required power at the airspeed for best endurance is reached. Until here, the power consumption of the propeller is caused by its profile power. At mid to high-speed, the pusher propeller is used for propulsion and thus unloads the main rotor from its propulsive force. Overall, the total power for Candidate 1 and Candidate 2 is very similar at high-speed. Candidate 1 consumes more total power at hover compared to Candidate 2 due to the additional tail rotor. However, due to the simplification of two isolated rotors without aerodynamic interactions for Candidate 2, the difference in total power is expected to be lower in reality as depicted. Furthermore, it is expected, that in reality Candidate 2 consumes more parasitic power at high-speed than depicted due to the larger rotor hub.

In order to find the best configuration, an evaluation matrix with various criteria has been defined to compare Candidate 1 and Candidate 2. For the evaluation, each criterion has been weighted with a numeric value, depending on its relevance (Table 2). Next, each candidate has been evaluated separately between DLR and AHTech with a numeric value

(Table 2). The evaluations of each criterium have been averaged, multiplied by the weight and summarized to select a configuration.

Table 2: Quantification of evaluation metric

Value	Weight	Evaluation
1	Very unimportant	Major disadvantage
2	Rather unimportant	Minor disadvantage
3	Neutral	Neutral
4	Rather important	Minor advantage
5	Very important	Major advantage

The criteria are divided into the following topics:

- Availability of the technology (Engine, gear-box, etc.)
- Complexity of the technology (Engine, gear-box, etc.)
- Flight performance (maximum airspeed, efficiency hover, efficiency high-speed, etc.)
- Flight control systems (complexity of algorithms, agility, etc.)
- Miscellaneous (development risk, etc.)

For example, the evaluation of the efficiency in fast forward flight differs for the candidates. The contribution of the rotor hub and shaft of a conventional helicopter can sum up to 35% of the total parasitic drag [10]. The resulting parasitic power rises cubically with airspeed, which is disadvantageous for the efficiency. The two rotor heads of the intermeshing rotor of Candidate 2 are expected to possess even higher parasitic drag. Therefore, Candidate 1 has been rated better in this criterion than Candidate 2.

The result of this analysis is that Candidate 1 performs slightly better than Candidate 2. This is based on the fact, that both thrust-compound configurations have a comparable design with similar design parameters. Single components differ significantly, but the major components (main rotor, pusher) are placed at similar positions with similar dimensions. As a result, Candidate 1 has been selected for the further detailing.

3. SYSTEM DESIGN

A system architecture has been defined for the FaUSt-Demonstrator, which divides the entire aircraft system into multiple subsystems (main rotor, main gear, fuselage, etc.). Next, the subsystem requirements have been derived from the aircraft re-

quirements and the predesign of the subsystems has been conducted with the focus on the lift, propulsion and drive systems. Figure 3-1 shows a cut-away depicting the external and internal arrangement of the system and subsystems. One aim of the arrangement is to place the center of gravity (CG) in the area underneath the main rotor.

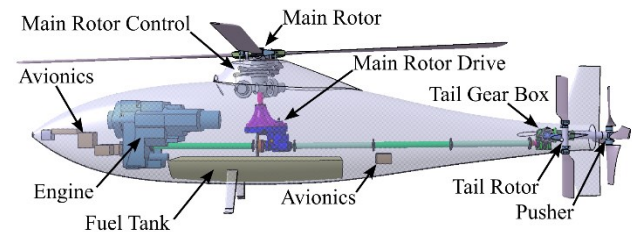


Figure 3-1: External and internal arrangement of the system and subsystems

3.1. Power Train

The operation of VTOL-UAVs in high-speed requires powerful engines due to the cubic rise of parasitic drag. After detailing the concept configuration, an engine with a Maximum Continuous Power (MCP) of at least 295 kW plus a reserve for uncertainties and auxiliary systems is needed for the FaUSt-Demonstrator. One possibility would be to use piston engines which are sometimes used on smaller helicopters, however, the poor power to weight ratio disqualifies them for the FaUSt-Demonstrator. Therefore, a turboshaft engine is required. The selection of Commercial Off-The-Shelf (COTS) engines is very limited between small UAVs and large manned helicopters and the development of a new turboshaft engine with a Full Authority Digital Engine Control (FADEC) exceeds the possibilities of the project.

As a result, an oversized COTS turboshaft engine has been selected for the FaUSt-Demonstrator. The disadvantages (high mass, large assembly space, suboptimal operating condition) are accept to enable manufacturing in a potential follow-up project. A single engine configuration is chosen, which offers lower weight, fuel consumption and costs compared to a multi-engine configuration. In addition, this approach simplifies the mechanical power transfer through the main gearbox. However, the capability to continue a flight in One Engine Inoperative condition (OEI) is not available.

The proposed engine has a maximum power of more than 480 kW. Additionally, this engine offers the possibility of both installation directions (air inlet

of engine in or against direction of flight), as the power shaft can be installed at the front or the rear of the engine. In the current configuration, the engine is located in front of the gearbox in terms of CG location, whereby the air inlet is located in flight direction and the power shaft is connected to the rear output of the engine.

The main gearbox includes one input for the engine shaft as well as two outputs for the main rotor and tail drive shaft (Figure 3-2), that is driving the tail and pusher gearbox. The main gearbox reduces the rotational speed from the engine to the required main rotor speed via a two stage gear train, consisting of one bevel gear and one helical gear stage. For the output to the tail drive shaft, connecting the main and tail gearbox, the rotational speed is not reduced and input and output shaft are coaxial to each other.

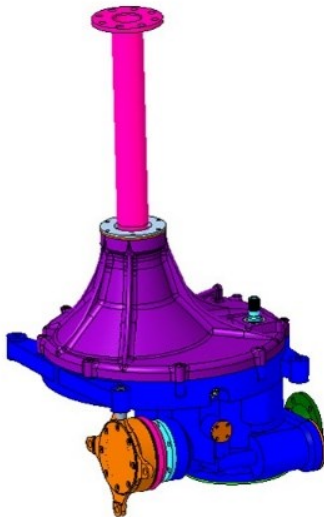


Figure 3-2: Concept of main gearbox

The position of the main gearbox is defined by the axis of the main rotor and the axis of the engine output shaft. Therewith, it is located near the design CG. Additionally, the main gearbox drives required accessories, such as a cooling fan for oil cooling of gearbox and engine and an alternator for electrical power generation.

The tail gearbox consists of one input and two outputs, one to the pusher and one to the tail rotor (Figure 3-3). The rotational speeds are reduced by a one stage helical gear train to the pusher and furthermore by an additional bevel gear on the pusher shaft reducing the speed to the required tail rotor

speed and providing 90° axis angle between pusher and tail rotor.

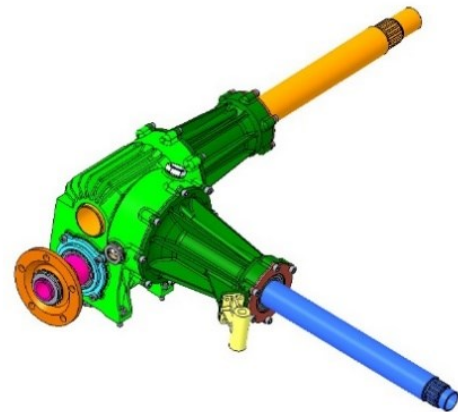


Figure 3-3: Concept of tail gearbox

The location of the tail gearbox is defined by the axis of the pusher and the axis of the tail rotor. Both gearboxes are connected via a tail drive shaft, which is a shaft currently split in three parts. Between each part, a coupling shall be installed in order to compensate occurring vibrations and movements of the tailboom of the aircraft. This is a common approach in helicopter applications. All power train components are designed based on technology and solutions, that have been proven their suitability and reliability, e.g. for CS-27, CS-29 or tilt-pro applications.

3.2. Main Rotor

A four bladed hingeless rotor system with a diameter of 5 m is chosen for the main rotor, considering disc and blade loading (Figure 3-4). The design parameters for the sizing rules were identified with respect to the high-speed requirement and the ability to manufacture a high-performance rotor with these dimensions. The design of the hub and blade attachments are more challenging compared to a fully articulated rotor system, but it benefits from less mechanical parts resulting in a lighter and easier production of the UAV. Furthermore, this rotor system is aerodynamically cleaner and causes less parasitic power, which is very beneficial for the intended operation at high-speed. Lastly, the hingeless rotor system improves the agility of the aircraft. The maintenance costs could be further reduced for a commercial product with a bearingless rotor system, but the additional design effort is not considered justifiable for a technology-demonstrator.

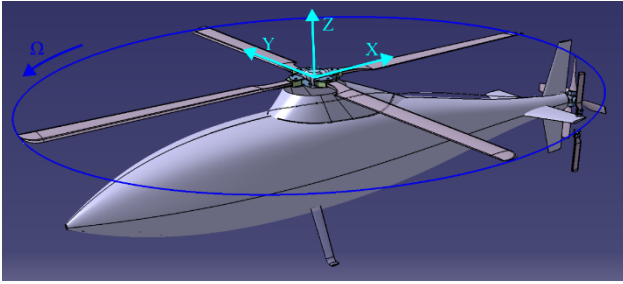


Figure 3-4: Concept of main rotor system

A plain blade design is used with respect to potentially building a technology-demonstrator and the usage of non-proprietary airfoils. The blade features a constant chord of 0.21 m up to a parabolic tip area, that starts at 92% of the radius. The aerodynamic shape begins at 22% of the blade and features a linear twist of $-8.0^\circ/R$. The tip itself is untwisted. Only a NACA 23012 airfoil is integrated, resulting in only geometric twist. The chord length at the tip is reduced to 0.105 m, which corresponds to 50% of the blade root chord.

The main rotor is operated at constant rotational speed of 80 rad/s and a blade tip speed of 200 m/s, which is slightly lower than that of a typical conventional helicopter. This corresponds to an advance ratio of 0.463 at 92.6 m/s airspeed or 0.5 at 100 m/s airspeed. Note that advance ratio of 0.5 is usually quoted as the maximum value for a conventional helicopter [14].

In general, a reduction of the tip speed is beneficial at high-speed to avoid transonic issues at the advancing blade and to fly faster. However, the loss of dynamic pressure and therefore the increased dissymmetry of lift must usually be compensated to avoid retreating blade stall. This could be done by other aircraft configurations with additional wings or by the use of the advancing blade concept (ABC, intermeshing or coaxial rotors) to reach an even higher airspeed. An optimization of the blade geometry by integrating better suited airfoils and applying a more sophisticated blade planform (e.g. combination of forward and backward sweep) will delay aerodynamic borders but not avoid them.

3.3. Tail Rotor

A two bladed seesaw rotor with a diameter of 1.14 m is selected for anti-torque and yaw-control (Figure 3-5). It is placed approximately at the height of the pusher shaft without tilt angle. The hinge possesses a δ_3 angle of 45° to couple the pitch-flap

motion, which causes a reduction of cycling flapping. As a result, the use of lead-lag hinges is avoided, which saves weight.

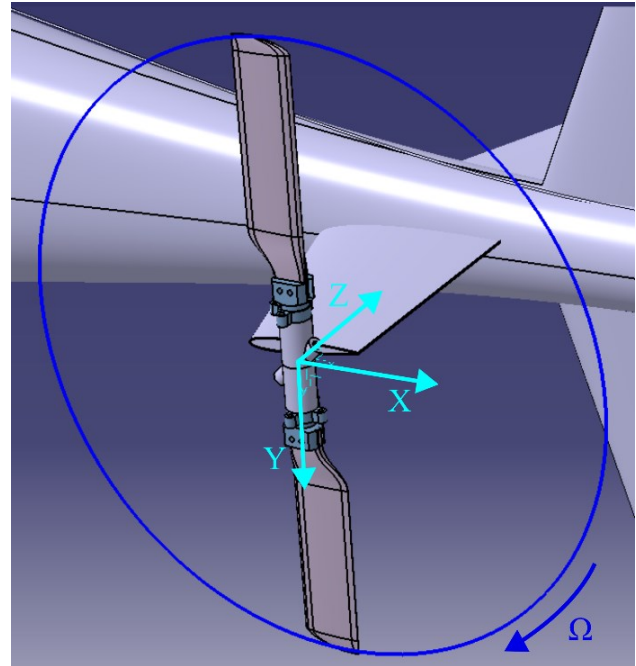


Figure 3-5: Concept of tail rotor system

The blade design includes an untwisted rectangular rotor blade with constant chord of 0.11 m and a parabolic tip at 95%, which reduces the chord to 33%. The symmetrical NACA 0012 airfoil is used. Similar to the main rotor, the blade tip speed is slightly reduced to 202.4 m/s to avoid transonic issues. This corresponds to a constant rotational speed of 355 rad/s.

3.4. Pusher Propeller

The pusher propeller is used for propulsion in high-speed with a diameter of 0.99 m and consists of four propeller blades (Figure 3-6). It is located at the rear of the fuselage without tilt angle at the height of the design CG to avoid undesired pitching moments.

The first blade design consists of a trapezoidal rotor blade with a hyperbolic twist of $-11,44^\circ \Theta/R$. It is tapered from 0.15 m at the blade root to 0.1 m at the blade tip. Compared to the main and tail rotor, a higher blade tip speed of 244 m/s is feasible due to the perpendicular inflow at forward flight. This results in higher thrust at a constant rotational speed of 493 rad/s. A negative sense of rotation is chosen to counteract the hanging sideward characteristics during trimmed forward flight.

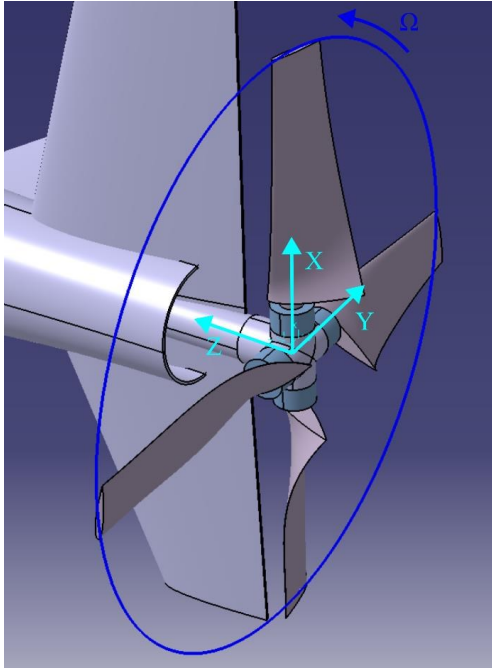


Figure 3-6: Concept of pusher propeller system

3.5. Main Rotor Control

Manned helicopters of this size and moderate maximum airspeed can often still be controlled without any power boosted control system. Because of the fact, that the FaUSt-Demonstrator is a UAV, it requires a full-authority fly-by-wire system and a state-of-the-art Automatic Flight Control System (AFCS). Due to the small size of the rotor system and the corresponding scaling laws, a swashplate-less control system, which would have provided the full range of Individual Blade Control (IBC) functionalities, was not an option in this case ([15], [16]). Therefore, a layout was chosen in which the actuation components are mounted within the fuselage and the control motions are transferred into the rotating frame via a conventional swashplate arrangement. This allows to use the classical three control input (collective, longitudinal cyclic and lateral cyclic). To simplify the operation and avoid the handling of pressurized hydraulic fluid, it was decided early in the design process to use full-electric actuation (Electric Mechanical Actuator, EMA) for all three control paths, namely main rotor, tail rotor and pusher.

Since the reliability requirements depend upon the legal framework under which the target vehicle will eventually be operated, it seemed to be worthwhile to look for actuator designs that were conceptually capable of being certified to the standards of

manned rotorcraft. A stringent proof of the corresponding safety level will, however, not be required for the operation under a Specific Operations Risk Assessment (SORA) flight permit of the EASA as foreseen for the FaUSt-Demonstrator. Therefore, the actuation system will be based on a dual-duplex, velocity summing EMA variant that has been developed for a 600 kg rotorcraft. Due to the typical oversizing as driven by the civil certification requirements, this actuator will be strong enough to safely control also the heavier and faster FaUSt-Demonstrator. Figure 3-7 shows the preliminary arrangement of the three main rotor actuators. Short connecting rods and single bell-crank levers are used to optimize the actuator packaging and to match the particular force - stroke requirements.

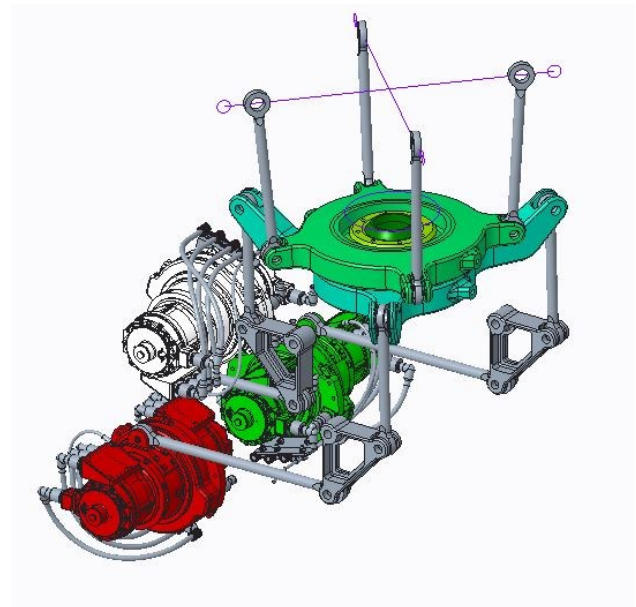


Figure 3-7: Concept of the main rotor control system

3.6. Tail Rotor Control

In addition to the main rotor controls, the FaUSt-Demonstrator will feature two more blade pitch control systems, one of them being the traditional tail rotor collective, primarily used to trim the tail rotor thrust in order to produce the required flight-condition-dependent amount of anti-torque. The other one being the collective of the thrust propeller. Due to the intended unloading of the main rotor in high-speed forward flight, the tail rotor thrust setting will often be lower than usual and agile yaw control will occasionally require even negative thrust. Figure 3-8 shows the principle arrangement of that pitch control mechanism. The required control motion is transferred via a single control rod that is guided

within the hollow tail rotor shaft. This keeps the tail rotor shaft free from any surrounding components and helps to realize an undisturbed horizontal stabilizer profile.

Due to the restricted space in the tail area and the disadvantage of high masses far rear of the overall CG, it has been decided to collocate the tail rotor with the main rotor pitch control actuators in vicinity of the main gearbox. The preliminary design uses a Flexball cable connection between the actuator and the ball crank at the end of above control rod.

The actuation will be based on the same EMA as used for the main rotor. The level of the Aircraft Functional Hazard Assessment (FHA) will reveal whether a dual-redundant architecture would be sufficient in this application and only one half of that actuator needs to be installed. In this case, the 50% loss of output rate could be recovered by trading in part of the torque capability through a suitable gear ratio.

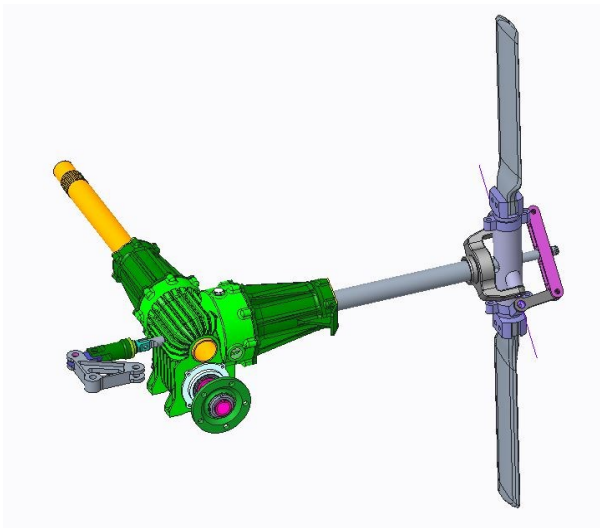


Figure 3-8: Concept of the tail rotor control system

3.7. Pusher Control

To optimize the flight-condition-dependent unloading of the main rotor by relieving it from the propulsive force component, the thrust setting of the pusher propeller must be adjustable. Since the pusher will be propelled via a mechanical drive train at a more or less constant rotational frequency, the only way of varying the pusher thrust is again collective pitch control. Figure 3-9 shows the principle layout of the corresponding mechanism. Based on the intended missions, however, the current vehicle design does not foresee the requirement for rapid thrust changes

as one would consider to use in a manned aircraft in order to improve agility. Thus, the control bandwidth of the pusher pitch control can be kept much lower than that of the rotors. Moreover, erroneous thrust settings in the longitudinal axis are less critical, which both justifies the application of a smaller and lighter COTS-derived EMA.

Due to the design of the power split in the tail gearbox, the propeller shaft cannot internally house an coaxial control rod. Therefore and unlike with the tail rotor control, the blade pitch links for the pusher control will be guided outside the propeller shaft to a gliding sleeve which in turn is moved by a control lever mounted in the non-rotating frame. The location of the actuator has not yet been finalized but will depend upon chosen variant. If size and weight permit, a position close to above control lever would be preferred.

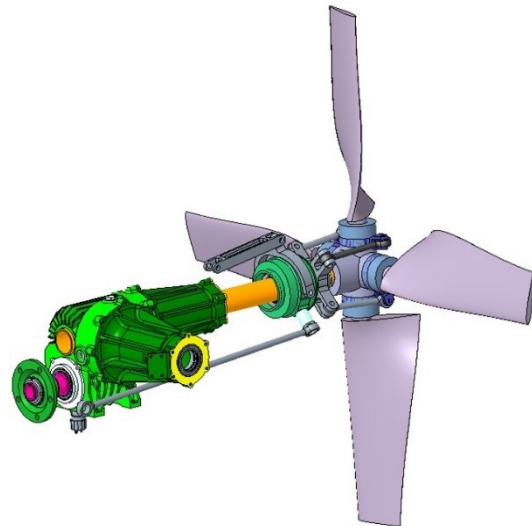


Figure 3-9: Concept of the pusher control system

3.8. Avionics

Since the FaUSt-Demonstrator is designed to solely demonstrate the high-speed flight performance, the avionics capabilities are focused on the flight test itself. Therefore, the main challenges of the flight test will be explained briefly:

- High-speed flight tests would be conducted with Beyond Visual Line of Sight (BVLOS) capable direct control by the remote pilot. Since the visual range is limited and the air-speed is high, a BVLOS system would be used to take over the aircraft in case of a problem.

- Utilization of different flight control modes during flight test and development. A direct control method is needed for first flight tests and as a flight test backup in case of technical issues for higher control modes. A control mode for In-flight closed-loop identification is needed for flight envelope expansion after an initial autopilot was successfully implemented for a slow airspeed.

Generally, the avionics are split between a flight safety-critical and a non-flight safety-critical part (Figure 3-10). In the flight-critical part of the avionics, the Flight Control Computer (FCC) is the main device for command and control. As an interface to the ground, a FaUSt-specific solution is implemented with a remote control interface, that allows for low-latency video to be transferred from the aircraft to the ground. Additionally, a C²-Datalink is used to send the control commands to the aircraft and receive flight information, as well as flight test data, back on the ground. Both the video and datalink facilitate the BVLOS capability. On the ground, a cockpit-like environment is used for the remote pilot to enable direct control.

The non-flight safety-critical part of the avionics consists of several devices, one of them being the Flight Test Instrumentation (FTI) to measure all flight test data. Another device is the aircraft interface computer. This computer is used to interface auxiliary systems like oil cooling or lighting.

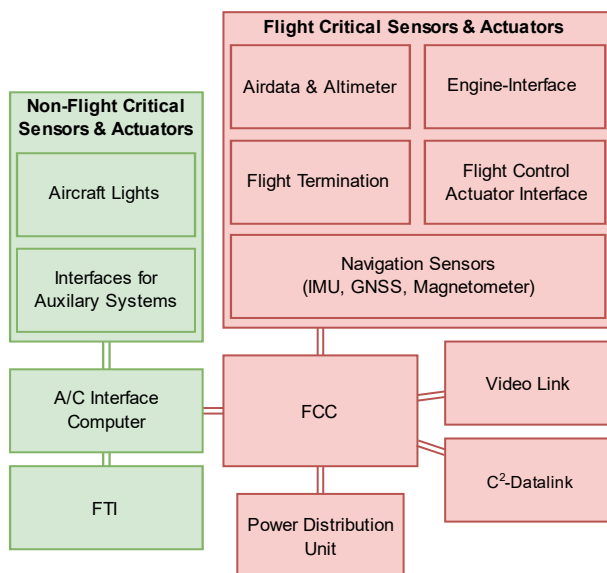


Figure 3-10: Overview of the avionics with flight critical parts in red and non-flight critical in green

4. FLIGHT PERFORMANCE

For the preliminary design, various flight conditions have been simulated to estimate the aircraft loads. This flight performance analysis has been updated continuously to verify the aircraft and subsystems requirements.

Table 3 shows the test matrix with all flight conditions that have been simulated. For each test point, a trim sweep was conducted according to the prescribed limits. The derived aircraft loads were based on stationary flight conditions and did not contain any dynamic aircraft loads. The forward flight trim sweep was performed for an airspeed between 0 and 100 m/s. As already mentioned, the maximum airspeed for the simulations is increased to 194 kt \approx 100 m/s to consider simulation uncertainties and to give a substantial speed margin. To be able to estimate the aircraft loads due to different load factors, steady right and left turns were performed with a bank angle between 0 and 47° resulting into a load factor between 1 and 1.5g. In order to meet the requirements defined for climb flight, trim sweeps with different climbing rates between 0 and 10 m/s were performed

Table 3: Test matrix of flight conditions

Test Point	Flight Conditions	Limits
1	Forward Flight	0 – 100 m/s
2.1	Steady Right Turn, 25 m/s	1 – 1.5g
2.2	Steady Right Turn, 35 m/s	1 – 1.5g
2.3	Steady Right Turn, 45 m/s	1 – 1.5g
3.1	Steady Left Turn, 25 m/s	1 – 1.5g
3.2	Steady Left Turn, 35 m/s	1 – 1.5g
3.3	Steady Left Turn, 45 m/s	1 – 1.5g
4.1	Steady Climb, 25 m/s	0 – 10 m/s
4.2	Steady Climb, 35 m/s	0 – 10 m/s
4.3	Steady Climb, 45 m/s	0 – 10 m/s

The steady turns and the climb flight trim sweeps were conducted for the airspeed 25, 35 and 45 m/s because the demonstration of maneuverability is performed in the range of lowest total power in forward flight (Figure 4-1). In the next section, only the results of the forward flight trim sweep are exemplary shown.

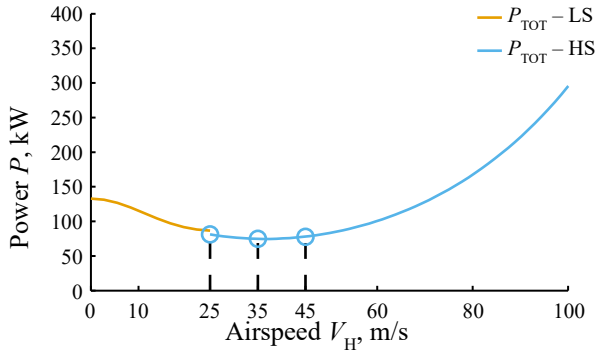


Figure 4-1: Total power curve with the test points of the maneuver flight (LS – low-speed, HS – high-speed)

4.1. Forward Flight Trim

To fully define a trim law, the number of free and fixed trim values has to be equal. For conventional helicopters, usually the three translational accelerations \dot{u} , \dot{v} and \dot{w} and the three angular accelerations \dot{p} , \dot{q} and \dot{r} form the fixed values and are set to be 0. The free trim values are the pitch and roll angle θ and φ and the four control inputs: collective (DDZ), longitudinal (DDM), lateral (DDL), and yaw input (DDN). To fulfill the requirements of the fixed trim values, the free trim values are varied until a steady trim state is reached. For the trim sweeps of the FaUSt Demonstrator, two different trim laws have been used because the forward thrust is generated differently depending on the airspeed.

In the hover and low-speed region ($V_H < 25$ m/s, Table 4), the main rotor generates forward thrust due to an increase of the pitch angle θ and the pusher is set to idle.

Table 4: Trim Law "Low-Speed" ($V_H < 25$ m/s)

Free	θ	φ	DDZ	DDM	DDL	DDN
Fixed	\dot{u}	\dot{v}	\dot{w}	\dot{p}	\dot{q}	\dot{r}

In the high-speed region ($V_H \geq 25$ m/s), the second trim law was used (Table 5). In contrast to the low-speed region, the pitch angle θ is set to 0° to minimize fuselage drag and the pusher is activated to generate forward thrust. Therefore, the pusher control input DDT has to be considered as a free trim value and replaces the pitch angle θ . The resulting trim values of the pitch and roll angle θ and φ are shown in Figure 4-2.

Table 5: Trim Law "High-Speed" ($V_H \geq 25$ m/s)

Free	DDT	φ	DDZ	DDM	DDL	DDN
Fixed	\dot{u}	\dot{v}	\dot{w}	\dot{p}	\dot{q}	\dot{r}

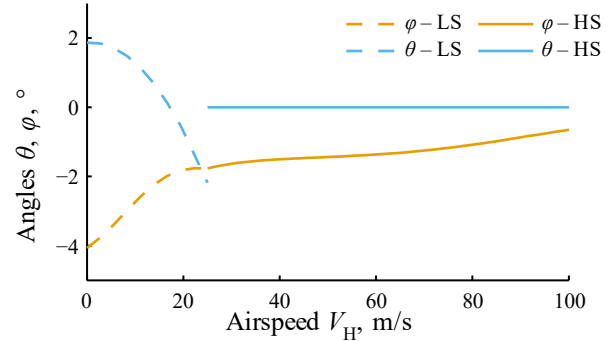


Figure 4-2: Trim values of the pitch and roll angle θ and φ (LS – low-speed, HS – high-speed)

Figure 4-3 shows the power distributions in total and for every propulsion system of the FaUSt-Demonstrator. The power distributions show the expected behavior as the main rotor is unloaded of the forward thrust in high-speed forward flight. Because the main rotor consequently needed lower torque, the tail rotor followed this behavior and produced correspondingly less anti-torque. The forward thrust was mainly generated by the pusher rotor, whose required power increases proportional with the airspeed.

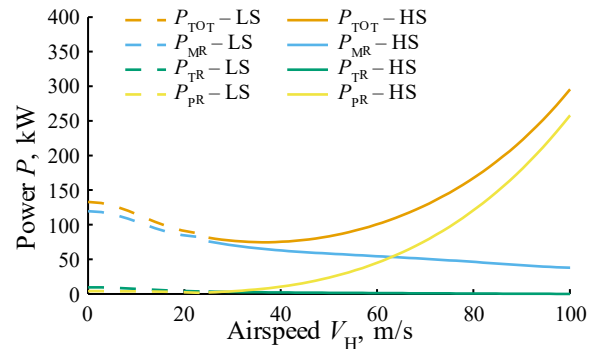


Figure 4-3: Power distribution of different components (total power (P_{TOT}), power main rotor (P_{MR}), power tail rotor (P_{TR}), power pusher (P_{PR}) / (LS – low-speed, HS – high-speed)

A variation of the flight mass leads mainly to changed required power during hover and low-speed as shown in Figure 4-4. Because the required power during high-speed is dominated by overcoming the aerodynamic drag, change in flight mass is only of secondary importance. However, the required power during hover and low-speed is domi-

nated by the induced drag, which is largely defined by the flight mass.

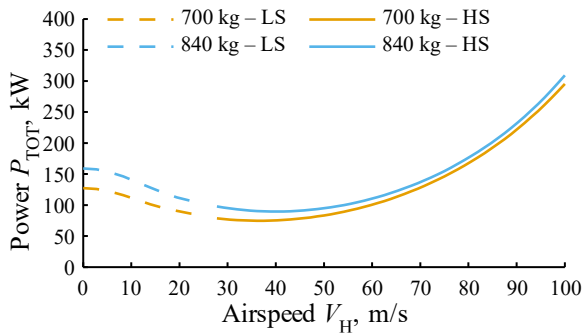


Figure 4-4: Power distribution in forward flight for different flight masses (LS – low-speed, HS – high-speed)

Figure 4-5 to Figure 4-7 visualize the distributions of selected parameters on the rotor disk at 100 m/s airspeed. The advancing blade is located at $\Psi = 90^\circ$ and the retreating blade at $\Psi = 270^\circ$.

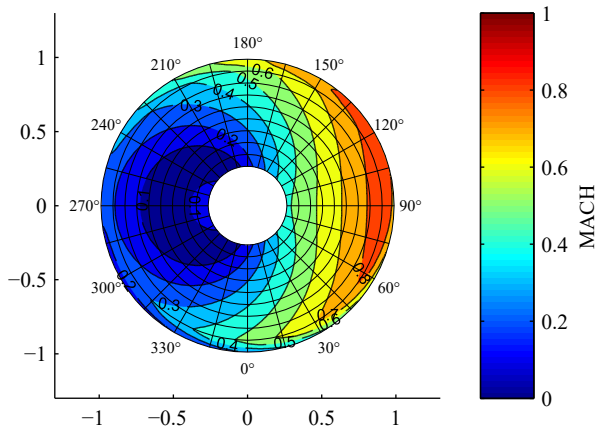


Figure 4-5: Mach number at 100 m/s airspeed at the rotor disk

Figure 4-5 shows the Mach number distribution on the rotor disk at 100 m/s airspeed. On the advancing blade between 60° to 140° , Mach numbers above 0.8 are reached. In the region of the retreating blade the Mach number is below 0.3, where for a rotor radius smaller than 75% the Mach number is even 0. Within an area of the retreating blade described by a rotor radius smaller than 25%, a small increase in Mach number from 0 to 0.1 can be identified because the blade in this area is impinged from behind.

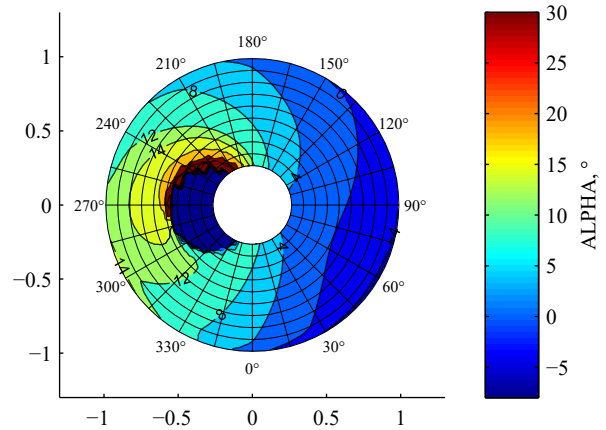


Figure 4-6: Angle of attack α at 100 m/s airspeed at the rotor disk

To achieve an equilibrium condition at highly unsymmetrical flow with an advance ratio of 0.5, the lift on the advancing blade has to be strongly reduced by cyclic control. This results in large areas of negative angle of attack α (Figure 4-6). At the retreating blade, areas with an angle of attack above 14° indicate an incipient stall, which, in reverse, means that no further lift can be generated.

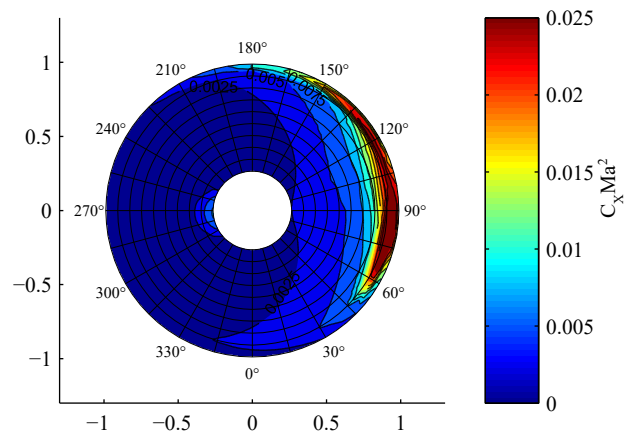


Figure 4-7: $C_x Ma^2$ at 100 m/s airspeed at the rotor disk

In combination with the local drag coefficient C_x scaled by the square of the Mach number Ma , a jump of the local drag coefficient by the Mach number Ma can be identified at the advancing blade between 60° to 150° at the last 20% of the rotor radius (Figure 4-7). The sudden increase of the local drag can be interpreted as supersonic shock areas.

4.2. Endurance and Range

The Specific Fuel Consumption (SFC) characteristics of the selected COTS engine have not been

available for the calculation of endurance and range. Therefore, an analytical fuel consumption model has been calibrated based on data of different engines available and suited for the installation in the demonstrator. The resulting maximum installed power for 30 s Super Contingency Power (SUP) is 621 kW with a SFC of 95 kg/GJ. The MCP condition of the model is at 72% of the SUP and has an SFC of 97.6 kg/GJ. The SFC as a function of the engine power is shown in Figure 4-8 for the case altitude mean sea level and an International Standard Atmosphere (ISA) temperature of 15°C.

Depending on the flight condition, the FaUST-Demonstrator operates with a mechanical power between 75 to 295 kW (Figure 4-3). The engine operates not at its optimal operating condition, which results in a reduction of endurance and range. As already mentioned, this is the consequence of the selection of a COTS unit instead of a virtual turboshaft engine.

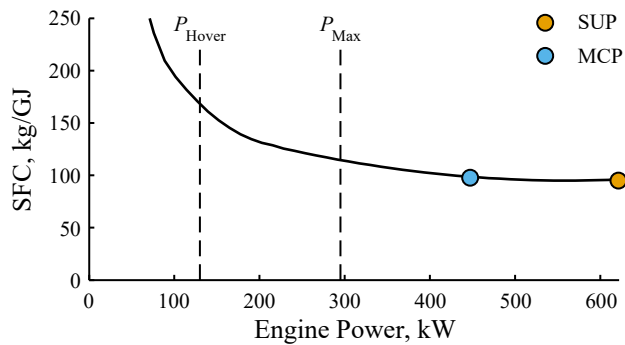


Figure 4-8: Specific Fuel Consumption (SFC) over engine power

A mission performance computation has been conducted with the flight model of the FaUST-Demonstrator and the calibrated engine model. In advance, the characteristic velocities have been computed from the performance curves considering flight masses ranging from 550 kg to 840 kg shown in Figure 4-9. The maximum airspeed of 100 m/s is achievable at all flight masses. The velocity for best endurance ranges from 32 m/s to 40 m/s with increasing flight mass. Although the best aerodynamics, or rather the glide number increases, the velocity best range, which is the combination of glide number and SFC, slightly decreases over the mass from 81 m/s to 79 m/s.

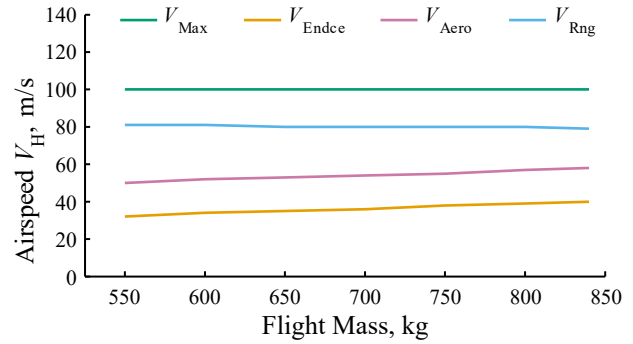


Figure 4-9 Characteristic velocities for different flight masses

Beyond the examination of performance parameters, a flight performance simulation has been conducted. Figure 4-10 shows range and endurance of the FaUST-Demonstrator with a fly-away mass of 700 kg and 840 kg. In both cases a fuel burn of 144 kg is simulated. With 700 kg and at a velocity of 80 m/s, the maximum achievable range is computed with 470 km. Flight time is 98 min. With a mass of 840 kg, the maximum range at 80 m/s decreases to 460 km with a flight time of 96 min. The highest endurances are achieved at 35 m/s with 134 min for 700 kg and 39 m/s with 128 min for 840 kg.

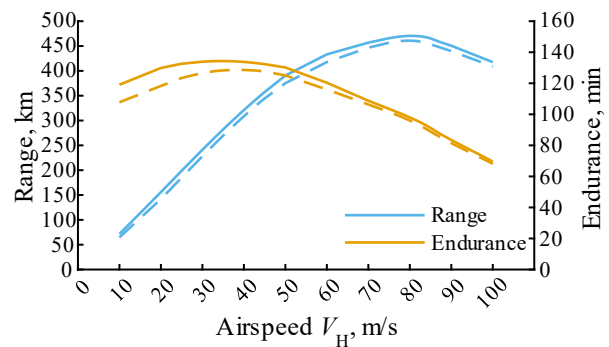


Figure 4-10: Dependence of endurance and range on airspeed (ISA sea level, 700 kg – solid, 840 kg – dashed)

The computation of the characteristic performance parameters and the mission simulation considering the actual fuel burn show very good agreement. Besides of the bad efficiency of the engines, due to the large amount of reserve power, the effective range is with possible 470 km quite high for unmanned configurations. The primary reason is the large fuel fraction of 20% of the fly-away mass, which is untypical even for conventional rotorcraft.

5. DISCUSSION

The design of the FaUST-Demonstrator aims to demonstrate the core flight performance capabilities by flight tests in a potential follow-up project. In addi-

tion, a balance between required flight performance and technological effort is kept. A variety of decisions have been made in favor of a sole technology-demonstrator. As a result, the design of the FaUSt-Demonstrator will not possess the full capability of a highly optimized commercial product, but rather serves as a proof-of-concept. In the following, the most relevant design decisions, their impact and possible improvements will be discussed:

1. **Technology-Demonstrator:** The feasibility of the concept shall be shown with a technology-demonstrator. Thus, the design focuses on the core capability (maximum airspeed ≥ 180 kt, adequate hover efficiency) with available technology instead of performing specific mission sizing of the aircraft with virtual components. Consequently, the FaUSt-Demonstrator might not possess the required payload and fuel capacity to operate with current military helicopters of the Armed Forces of Germany. But the concept of the lift, propulsion and power train systems will be fully transferrable to a commercial product. Furthermore, other aspects of a potential commercial product (e.g. autorotation, interaction with manned helicopters, etc.) are not fully covered by the demonstrator.
2. **Engine:** The selection of a COTS turboshaft engine enables the manufacturing of the FaUSt-Demonstrator in a potential follow-up project. Due to the oversized power, an increased mass and assembly space is needed, which dominates the cross-sectional area of the fuselage. Furthermore, the engine is used far outside of the optimal operating condition, which causes an increased fuel consumption and a reduction of endurance/range. It can be expected, that a commercial product would grow in mass and size, which would move the operating condition of the same engine towards more efficiency. Furthermore, a modification of the COTS turboshaft engine to shift the optimal operating condition might be possible.
3. **Optimization Lift/Propulsion:** Intensive optimization of the lift and propulsion systems has been waived, because complex blade geometries or proprietary airfoils are not needed for the demonstration of the concept. It can be expected, that the maximum

airspeed could slightly be increased by further optimization of those systems.

4. **Stub Wings:** Military rotorcrafts often use stub wings without ailerons to carry additional mission equipment such as auxiliary fuel tanks. For a thrust-compound configuration such as the FaUSt-Demonstrator, stub wings could unload the main rotor even further by lift, which results in a slight increase of the maximum airspeed. Adverse effects would be a decrease in hover efficiency and an increase of parasitic power.
5. **Faster Configuration:** If a medium increase of the maximum airspeed is needed, it would be possible to increase the technological effort and to enhance the candidate configurations from the concept investigation. Candidate 1 could be developed into a lift-compound configuration by adding wings to unload the main rotor. In contrast to plain stub wings, more complex wings with ailerons are required for sufficient control power at high-speed. However, these would again decrease hover efficiency. Candidate 2 could be developed into a combination of the intermeshing rotor with the ABC design. This approach requires two very rigid rotors and tends to suffer from vibrations. It can be expected, that the additional technological effort of both enhanced configurations is needed for a maximum airspeed of approximately more than 220 kt. Due to the cubic rise of parasitic power with airspeed, those configurations tend to grow in mass and size to compensate the additional fuel consumption at very high-speed.

6. CONCLUSION

A concept study within the project FaUSt, showing the first results of the design of a fast VTOL-UAV technology-demonstrator for MUM-T, has been presented. The project aims to design of a VTOL-UAV, which is able to effectively operate with the current helicopters of the German Armed Forces without limiting the flight performance of the combined tactical unit. Particular attention is paid on the balance between required flight performance and technological effort. Therefore, the primary design objective has been a maximum airspeed of at least 180 kt with an adequate hover efficiency.

For this purpose, different candidate configurations have been defined, analyzed and evaluated. As a result, a thrust-compound configuration has been selected for the FaUSt-Demonstrator. A system architecture has been defined and the predesign of the subsystems have been conducted with focus on the lift, propulsion and drive systems. The flight mechanic model was updated continuously with the progress of the development to analyze the flight performance of the entire system. Based on the simulations results, the proposed design of the VTOL-UAV is expected to fulfill the requirements on the technology-demonstrator.

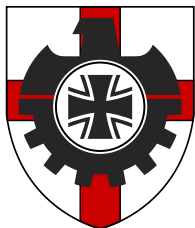
Future work within this project will focus on detailing the design of the technology-demonstrator. Due to the focus on available technology, the manufacturing, preflight testing in a simulator and flight testing on a test site in a potential follow-up project would be feasible.



Figure 6-1: FaUSt-Demonstrator at DLR's research flight simulator AVES

7. ACKNOWLEDGMENTS

The authors would like to thank the Federal Office of Bundeswehr Equipment, Information Technology and In-Service Support (BAAINBw L1.1) for funding the project.



8. REFERENCES

- [1] A. E. Voigt, A. Donkels and K. K. Fettig, "Manned-Unmanned Teaming Cooperative Formation Flight - A Project Review," in *Vertical Flight Society's 75th Annual Forum & Technology Display (VFS)*, Philadelphia, PA, USA, May 13–16, 2019.
- [2] J. Wartmann, A. Dikarew, K. Fettig, P. Petit, S. Seher-Weiß and A. Voigt, "System Identification of a Compound Intermeshing Rotor UAV," in *Vertical Flight Society's 79th Annual Forum & Technology Display (VFS)*, West Palm Beach, FL, USA, May 16–18, 2023.
- [3] M. J. Adriaans, R. C. Cribbs, B. T. Ingram and B. P. Gupta, "A160 Hummingbird Unmanned Air Vehicle Development Program," in *American Helicopter Society International Specialists Meeting on Unmanned Rotorcraft*, Chandler, AZ, USA, Jan. 23–25, 2007.
- [4] M. Hardesty, T. Berka, S. Kennedy, S. Dixon, J. Graham and D. Caldwell, "Unmanned Little Bird H-6U," in *American Helicopter Society International Specialists Meeting on Unmanned Rotorcraft*, Chandler, AZ, USA, Jan. 23–25, 2007.
- [5] B. Settle and T. Wise, "Bell Eagle Eye TR-911X - Tiltrotor Unmanned Aerial Vehicle: Recent Developments, Autoland Integration, And Flight Test Demonstrations," in *American Helicopter Society 56th Annual Forum (AHS)*, Virginia Beach, VA, USA, May 2–4, 2000.
- [6] S. Yu, J. Heo, S. Jeong and Y. Kwon, "Technical Analysis of VTOL UAV," *Journal of Computer and Communications*, vol. 4, no. 15, pp. 92-97, 2016.
- [7] C. A. Mitchell and B. J. Vogel, "The Canard Rotor Wing (CRW) Aircraft - A New Way to Fly," in *AIAA International Air and Space Symposium and Exposition: The Next 100 Years*, Dayton, OH, USA, July 14–17, 2003.
- [8] M. J. Hirschberg, "V/STOL: The First Half-Century," *Vertiflite*, vol. 43, no. 5, pp. 34-54, 1997.

- [9] B. G. van der Wall, Grundlagen der Hubschrauber-Aerodynamik, ISBN 978-3-662-44399-6, Berlin Heidelberg, Germany: Springer Vieweg, 2015.
- [10] J. G. Leishman, Principles of Helicopter Aerodynamics, Second Edition, ISBN 978-0-521-85860-1, Cambridge, UK: Cambridge University Press, 2006.
- [11] P. Weiland, M. Buchwald and D. Schwinn, "Process Development for Integrated and Distributed Rotorcraft Design," *MDPI Aerospace*, vol. 6, no. 2, 2019.
- [12] P. Weiland, D. Schwinn, R.-G. Becker, T. Weber, K. Atci, I. Moerland-Masic and F. Reimer, "Sizing of a New SAR Helicopter for a Future HEMS Environment," in *Deutscher Luft- und Raumfahrtkongress (DLRK)*, Dresden, Germany, Sep. 27–29, 2022.
- [13] B. Benoit, A.-M. Dequin, K. Kampa, W. von Grünhagen, P.-M. Basset and B. Gimonet, "HOST, a General Helicopter Simulation Tool for Germany and France," in *American Helicopter Society 56th Annual Forum (AHS)*, Virginia Beach, VA, USA, May 2–4, 2000.
- [14] R. W. Prouty, Helicopter Aerodynamics, ISBN 978-0972636865, Mojave, CA, USA: Mojave Books LLC, 2004.
- [15] U. T. P. Arnold, T. Auspitzer, J. Haar, C. Sutton and P. Bates, "Electric, Swashplate-less Individual Blade Control System to Be Wind Tunnel Tested in Full-Scale," in *45th European Rotorcraft Forum*, Warsaw, Poland, Sept. 17–20, 2019.
- [16] T. Auspitzer, J. Haar, U. T. P. Arnold, C. Sutton and J. O'Neill, "Development of a Pure-Electric, Swashplate-less Individual Blade Control System for a High Speed Rotor Configuration – Research Program Update," in *AIAA SciTech Forum*, San Diego, CA, USA, Jan. 3–7, 2022.